CONF-791135--8

X-RAY AND PRESSURE CONDITIONS ON THE FIRST WALL OF A PARTICLE BEAM INERTIAL CONFINEMENT REACTOR

by

G. R. Magelssen

Prepared for

Twenty-First Annual Meeting

Division of Plasma Physics

Boston, Massachusetts

November 12-16, 1979

ARGONNE NATIONAL LABORATORY, ARGONNE, ILLINOIS

Operated under Contract W-31-109-Eng-38 for the

U. S. DEPARTMENT OF ENERGY

X-RAY AND PRESSURE CONDITIONS ON THE FIRST WALL OF A PARTICLE BEAM INERTIAL CONFINEMENT REACTOR*

G. R. Magelssen

Argonne National Laboratory
Argonne, Illinois 60439

ABSTRACT

Because of the presence of a chamber gas in a particle beam reactor cavity, nonneutron target debris created from thermonuclear burn will be modified or stopped before it reaches the first reactor wall. The resulting modified spectra and pulse lengths of the debris need to be calculated to determine first wall effects. Further, the cavity overpressure created by the momentum and energy exchange between the debris and gas must also be calculated to determine its effect. The purpose of this paper is to present results of the debris-background gas problem obtained with a one fluid, two temperature plasma hydrodynamic computer code model which includes multifrequency radiation transport. Spherical symmetry, ideal gas equation of state, and LTE for each radiation frequency group were assumed. The transport of debris ions was not included and all the debris energy was assumed to be in radiation. The calculated x-ray spectra and pulse lengths and the background overpressure are presented.

* Work supported by Department of Energy.

1. Introduction

In a previous paper,[1] we discussed some of the reasons why and the conditions under which a form of protection is needed for the first wall of a inertial confinement reactor cavity. In that paper we used a simple target model (deuterium-tritium surrounded by mercury) to illustrate how the x-ray and charged particle spectra, pulse lengths and energies depended on the target yield, mass and density structure. This information, however, isn't adequate to design the particle beam reactor first wall. Reactor vessel pumping and driver focusing constraints put limits on the background cavity pressure. For example, to focus electron or 1-10 MeV particle energy - light ion beams may require pressures greater than 50 Torr, and heavy ions may require pressures either less than or equal to 10^{-4} Torr or around a Torr.[2,4]

Because of the presence of a chamber gas, nonneutron target debris will be modified or stopped before it reaches the first reactor wall. The resulting modified spectra and pulse lengths need to be calculated to determine first wall effects; i.e., sputtering, thermal stress, etc.. Further, the cavity overpressure created by the momentum and energy exchange between the debris and gas must also be calculated to determine its effect.

The purpose of this paper is to present results of the debris-background gas problem obtained with a one fluid, two temperature plasma hydrodynamic computer code model which includes multifrequency radiation transport.[5] Previous numerical approaches to this problem have used a one group (i.e., one temperature) radiation treatment.[2] Analytical estimates of the background gas overpressure have also been made.[6] To our knowledge, our model is the only one to treat multifrequency radiation transport. With such a treatment we can better estimate spectral and energy characteristics of the radiation incident upon the first wall and the overpressure created. Our model assumes spherical symmetry, ideal gas equation-of-state and LTE for each frequency group. The transport of debris ions was not included and all the nonneutron debris energy was assumed to be in radiation. The calculated x-ray spectra, pulse lengths, and the background overpressure are presented.

In our calculations the target spectra must be given as an initial condition. We could have used the published spectra from proposed reactor type targets.[7] However, because of the uncertainty associated with the target design and because of the sensitivity of the target spectra to the target yield and mass, we felt it would be useful to study the cavity problem using target spectra which represent significantly different spectral regimes. Our previous

work suggests three regions.[1] Using the ratio X ≡ Target Yield (MJ)/Target mass (mg) they are X ∿ 100, X ∿ 1, and X < < 1. The first region (i.e., X ∿ 100) corresponds to a solid, spherical bare deuterium-tritium target and isn't considered here. The latter two regions have significantly different spectral and pulse characteristics. For example, for X < < 1 the target x-rays are released in a few to many nsecs and have a "bulk" spectrum less than a 500 eV black body. Most of the nonneutron energy is in ions with only a few percent (i.e.≲ 1 to 3%) in x-rays. For X ∿ 1, the x-rays are released in a nsec or less with a "bulk" spectrum on the order of or greater than a 1 keV black body. More than half of the nonneutron energy is in x-rays.

The "bulk" spectrum is the radiation released after thermonuclear burn as a result of thermal and radiation conduction through the target. Some "nonbulk" high energy x-rays generated during thermonuclear burn pass through the target material without absorption. Their energy content is roughly a magajoule or less for a 150 MJ yield target, and the photons generally have energies greater than 30 keV. The pulse length of this hard x-ray burst is roughly the burn time, a few to a few hundred picoseconds. For more information about the target x-ray and ion spectra see our previous paper.[1]

The next section gives a discussion of our numerical model. In Section 3 we describe the target and background gas conditions considered. The results are presented in Section 4., which is followed by a summary and conclusions.

2. Numerical Model

The hydrodynamic-radiation transport model utilizes one-dimensional (planar, $\delta = 1$; cylindrical, $\delta = 2$; shperical, $\delta = 3$) Lagrangian coordinates. When using Lagrangian coordinates the spatial variable r can be replaced by the change of variable

$$dM_0 = r^{\delta-1} \rho(r)\, dr \qquad (1)$$

where M_0 is the new independent variable, the Lagrangian mass. Using this new independent variable, the one-fluid equation of motion is written as

$$\frac{\partial u}{\partial t} = r^{\delta-1} \frac{\partial}{\partial M_0} (P + Q) \qquad (2)$$

when u is the fluid velocity, $P = P_{electron} + P_{ion} + P_{radiation}$ is the total fluid pressure and Q is the von-Neumann artificial viscosity. This quantity

has non-zero values only in regions experiencing compression. It is inserted into this inviscid equation to add dissipation in regions undergoing shock propagation. This is a numerical expedient which allows a much more rapid solution of the equation without the appearance of numerical instabilities. The hyperbolic equation of motion is solved by using a standard explicit finite-difference technique.[8]

Although the plasma is treated as one fluid for the purpose of the equation of motion, it is assumed that the electrons and ions are in local equilibrium at their own temperatures. There are, therefore, two separate energy equations describing the fluid plasma. These are coupled by the electron-ion collisional equilibration term:

$$C_{Ve} \frac{\partial T_e}{\partial t} = \frac{\partial}{\partial M_o} \left(r^{\delta-1} Ke \frac{\partial T_e}{\partial r}\right)$$

$$- (P_e)_T \frac{\partial V}{\partial t} T_e - W_c (T_e - T_i) + S_e \qquad (3)$$

$$C_{Vi} \frac{\partial T_i}{\partial t} = \frac{\partial}{\partial M_o} \left(r^{\delta-1} Ki \frac{\partial T_i}{\partial r}\right) + W_c (T_e - T_i)$$

$$- (P_i)_T \frac{\partial V}{\partial t} T_i - Q \frac{\partial V}{\partial t} \qquad (4)$$

where C_{Vc} and C_{Vi} are the electron and ion specific heats, K_e and K_i are the electron and ion thermal conductivities, W_c is the electron-ion collisional coupling term, $(P_e)_T$ and $(P_i)_T$ are defined by $(P)_T \equiv \frac{\partial P}{\partial T}$ and S_e is the radiation source term for the electrons. For the calculations presented, the classical (Spitzer) forms of the transport coefficients were used. The electron temperature equation is flux limited so that fluxes no greater than the physically plausible free streaming limit will be allowed. Ideal gas equations of state are used to compute the pressures and specific heats. These coupled nonlinear parabolic equations are solved simultaneously by using an implicit Crank-Nicholson differencing scheme.[8] The nonlinear coefficients are evaluated explicitly.

The radiation transport is computed by using the multifrequency-variable Eddington technique. The radiation transport equation is expanded in angular moments, and the infinite set of moment equations truncated at two. These are given by:

$$\frac{\partial E}{\partial t} + \frac{1}{r^{\delta-1}} \frac{\partial}{\partial r} (r^{\delta-1} F) + c \sigma_a E = J \tag{5}$$

$$1/c \frac{\partial F}{\partial t} + c \left(\frac{\partial P}{\partial r} + \frac{\delta-1}{2r} (3P-E)\right) + (\sigma_s + \sigma_a) F = 0 \tag{6}$$

where E (r, v, t) and F (r, v, t) are the frequency-dependent radiation energy density and flux, respectively. The σ_s and σ_a are the scattering and absorption cross-sections and J (r, v, t) is the radiation emission function. The radiation tensor P (r, v, t) is, of course, specified by the higher order truncated moment equation. To complete the truncation procedure, this pressure must be approximated in terms of E and F. In the variable Eddington approximation the pressure is given by the semi-emphirical formula

$$P = f E \tag{7}$$

where f is the variable Eddington factor. This term has a lower limit of $f \to 1/3$ in regions of high opacity, implying an isotropic radiation distribution, and has an upper limit of $f \to 1$ in regions of low opacity implying free streaming radiation. With this model, radiation can be transported fairly accurately if its angular distribtuion is not a critical quantity. For the results presented, the angular distribution is not critical because the radiation originates at the center of the spherical chamber.

The radiation energy and flux equations are further reduced to multi-group form where a set of equations is solved for each frequency group. These equations take the form

$$\frac{\partial E^v}{\partial t} + \frac{1}{r^{\delta-1}} \frac{\partial}{\partial r} (r^{\delta-1} F^v) + c \sigma_a^v E^v = J^v \tag{8}$$

$$1/c \frac{\partial F^v}{\partial t} + c \left(\frac{\partial P^v}{\partial t} + \frac{\delta-1}{2r} (3P^v - E^v)\right) + (\sigma_a^v + \sigma_s) F^v = 0 \tag{9}$$

where

$$E^v (r,t) = \int_{v_m}^{v_{m+1}} E (r,v,t)\, dv \tag{10}$$

and similarly for the other quantities.

A fully implicit finite difference technique is used. The equations are solved for $E^{\nu}(r,t)$ and $r^{\delta-1} F^{\nu}(r,t)$ using the straight mean opacity in the energy equation and the Rosseland opacity in the flux equation. The radiation pressure which is the sum of the group pressures is coupled to the fluid motion, and the radiation energy exchange, which is the sum of each group's exchange, is coupled to the electron temperatures through the source term S_e.

The emission function J^{ν} is composed of two terms, R^{ν} and T^{ν}. T^{ν} is the radiation source term due to the target explosion and R^{ν} is the plasma radiation emission function. The opacity functions were taken from the Handbook of Spectroscopy.[9] Since LTE was assumed, the emission function R^{ν} was determined by Kirchhoff's law:

$$R(\nu) = B(\nu)\, \sigma(\nu) \qquad (11)$$

where $B(\nu)$ is the Planck function.

The equation of state is much simplified. Ideal gas laws were used and the plasma was assumed to be singly ionized. For the calculations presented, 25 to 50 spatial zones were used and each calculation required about 2000 time steps. Twenty frequency groups were used in the radiation transport calculation.

3. Chamber Gas and Target Conditions

It has been suggested that 100 Torr will be adequate to focus electron or light ion beams, and helium, neon, and argon have been considered as the background gas.[2-4] To our knowledge, no choices have been considered for heavy ions. However, Rutherford scattering of the heavy ions with the background gas may limit the choice to low Z materials.[10,11] In our calculations we considered neon.

The chamber size is an additional constraint. For a spherical chamber, a radius of 1-5 meters has been considered for electron and light ion beams.[2-4] The radii suggested for heavy ions is 5 to 10 meters.[12] In our calculations, the chamber radius was assumed to be 3, 5 or 10 meters and most calculations were done using a 5 meter radius chamber.

We have chosen the yield for all targets considered to be 150 MJ. This yield is compatible with the Solase study and with the yields suggested of electron and light ion drivers.[2-4;13] In order to consider the severest conditions imposed by nonneutron debris, we have assumed some neutron slowing down within the target. Calculations suggest that 30% of the thermonuclear

energy released could be in charged particles and x-rays.[14] As a result, we chose the nonneutron energy content to be 45 MJ. For $X << 1$ we chose the target x-ray spectra to be a 200 eV black body with a 10 nsec pulse. For $X \sim 1$, it was a 1 keV black body with a nsec pulse.

4. Results

For 100 Torr neon Fig. 1 gives the x-ray energy incident upon the first wall as a function of time. Figure 2 shows the overpressure as a function of chamber radius and time. The dotted curves are for $X << 1$. It can be seen from Fig. 1 that the x-rays are contained in three bursts. There is the hard x-ray burst which passes through the target and the chamber gas (i.e., the "nonbulk" part of the target spectra). Its energy content for a 150 MJ target is roughly a mJ and the photons generally have energies greater than 30 keV. This pulse is followed by a softer burst of longer duration. For $X << 1$ most of the energy content in this intermediate burst is contained in photons with energies from 6-15 keV (see Fig. 3). The pulse length is about 100 nsec and the energy content is 40 kJ. Figure 3 gives the time integrated x-ray spectra at the first wall for $X \sim 1$ and $X << 1$ approximately a millisecond after the target explosion. For $X \sim 1$ photons with energies from 6 - 30 keV contain most of the energy. The pulse duration is roughly 10 nsec and the x-ray content is 700 kJ.

The final burst has a much longer pulse and contains x-rays ranging in energy from 20 eV to less than 1 eV. Because we do not expect LTE to be valid when the plasma temperature drops below the first ionization potential of the gas, we do not expect our transport calculation to be accurate when a significant portion (i.e., 50%) of the hot chamber gas cools below the first ionization potential. The time when this occurs does, however, give a rough estimate of the lower limit to this long pulse. For our calculations this pulse length is about a tenth of a millisecond for both $X \sim 1$ and $X << 1$.

Figure 2 does not present a complete picture of the pressure pulse. The blast wave which creates the overpressure is reflected back and forth between the wall and the cavity center. The number of reflections between successive target explosions may be estimated crudely by using an acoustic approximation:

$$N \simeq \tilde{C}_s / p_s \cdot D$$

when $\tilde{C}_s$ is the average sound speed between pulses, D is the chamber diameter and ps denotes the number of pulses per second. For both $X << 1$ and $X \sim 1$, the pressure pulse arrived at the first wall, which was 5 meters from the chamber center, about 2 milliseconds after the explosion. The overpressure was 2 and 2.5 atmospheres for $X \sim 1$ and $X << 1$, respectively. For neon at 1 eV which is consistent with our results $\tilde{C}_s$ is approximately 2×10^5 cm/sec. For 10 pulses a second and a chamber of 5 meters radius, N = 20. In our calculations the second pulse arrived about 6 milliseconds after the explosion and the overpressure had decreased roughly 20 percent. The decrease was due mainly to an increase in the plasma internal energy.

Figure 4 gives the time-integrated x-ray spectra incident upon the first wall for a 3 meter radius chamber. This again is the spectrum one millisecond after the explosion and is the result for the case in which $X << 1$. The pulse length was 100 ns and the overpressure at the wall was 7 atmospheres.

Figure 5 gives the time dependence of the x-ray energy at the first wall for a one Torr neon-filled chamber and Fig. 6 shows the overpressure. The overpressure for the $X << 1$ and $X \sim 1$ cases was 3.5 and 0.3 atmospheres, respectively. The dotted curves are for $X << 1$. Again, the x-rays are contained in three bursts. There is the hard x-ray burst of very short duration which has already been discussed. One Torr neon is much less effective than 100 Torr in stopping x-rays. For $X << 1$ the energy content of this second burst was 1.2 MJ. Its pulse length was 200 ns and most of the energy was in 0.3 to 8 keV photons. As a result, the intermediate bursts contains significantly more energy. For $X \sim 1$ the energy content was 24 MJ, and the pulse length was 5 ns. Most of the energy was in 0.9 to 12 keV photons. The time integrated spectrum a millisecond after the explosion for both $X << 1$ and $X \sim 1$ cases are given in Fig. 7. Figure 8 gives a similar spectrum for a 10 meter radius chamber. For this calculation $X << 1$. The energy content was 357 kJ and most of the energy was carried by 2-6 keV photons. The over pressure at 10 meters was 0.3 atmospheres.

5. Conclusions

The x-ray spectra and energy content and the gas overpressure due to a target explosion in the center of a neon filled spherical chamber have been calculated using a hydrodynamic-radiation transport computer code. All the nonneutron debris was assumed to be in radiation and cavity pressures of 1 and 100 Torr were considered. Two significantly different initial target spectral x-ray conditions were studied. A 200 eV black body with a 10 ns pulse and a 1 keV black body with a 1 ns pulse were considered. The radiation

transport calculation was multifrequency and LTE was assumed for each frequency group. The initial x-ray energy content was 45 MJ.

Several general conclusions can be drawn from our results:

(1) The photons incident upon the first chamber wall are contained in three bursts:

i. A hard x-ray burst of short duration (i.e., $\lesssim$ 1 ns) which is created during thermonuclear burn and which passes through the target and chamber without absorption.

ii. A softer burst of longer duration, part of which is created by the absorption of debris near the target with the emission of x-rays that reach the wall and part of which comes from the target plasma "bulk" radiation that passes through the chamber without absorption. The "bulk" target radiation is x-ray energy released after thermonuclear burn as a result of thermal and radiation conduction through the target.

iii. A soft burst of long duration created by the radiation cooling of the entire chamber gas.

(2) As X (X $\equiv$ Target Yield in mJ/Target Mass in mg) decreases the energy content of the intermediate burst decreases.

(3) As X decreases the overpressure at the first wall increases.

Several specific conclusions can also be made. For X $\sim$ 1 we have calculated that both 100 Torr and 1 Torr neon filled 5 meter radius chambers can protect the first wall from soft x-rays (i.e., photons less than 1 keV) resulting from the intermediate burst. In the case of 1 Torr, however, the energy content in hard x-rays (i.e., photons greater than 1 keV) is quite large, 24 mJ for a target yielding 45 MJ of nonneutron energy. For X $<<$ 1 a 3 meter radius chamber at 100 Torr and a 10 meter chamber at 1 Torr can protect the wall from these x-rays.

Our results are significantly different from those previously published. Neither the hard nor the intermediate bursts described here have been discussed before. Our calculations suggest that it is not adequate to estimate just the absorption of target x-rays by the background cavity gas, or to use a one temperature radiation model. The dynamics of the radiation absorption and emission at all frequencies must be calculated to determine the x-ray spectra and flux, and the cavity overpressure at the first wall. Further, the plasma evolution and the radiation energy content, pulse length and spectra will depend not only upon the background gas type and pressure and the target yield, but the target yield to mass ratio which determines to a great extent the percent of energy, the pulse lengths and the spectra of the target x-rays and ions.

Acknowledgements

The author wishes to thank G. A. Mosses, J. J. Devaney, and M. A. Sweeney for several useful discussions.

References

[1] Magelssen, G. R. and Moses, G. A., Nucl. Fusion, 19 (1979) 301.

[2] Cook, D. L. and Sweeney, M. A., Proceedings of the Third Topical Meeting on the Technology of Controlled Nuclear Fusion, Vol. 2 (1978) 1178.

[3] Cook, D. L. and Sweeney, M. A., ANS First Topical Meeting on Fusion Reactor Materials (1979).

[4] Yonas, G., Seventh International Conference on Plasma Physics and Controlled Nuclear Fusion (1978).

[5] Magelssen, G. R., IBF Note #

[6] Freiwald, D. A. and Axford, R. A., J. Appl. Phys., 46 (1975) 1171.

[7] Varnado, S. and Carlson, G., Nucl. Tech., 29 (1976) 415.

[8] Richtmyer, R. D. and Morton, K. W., Difference Methods for Initial Value Problems, John Wiley, New York (1967).

[9] Robinson, J. W. (Editor), CRC Handbook of Spectroscopy, Cleveland, CRC Press (1974).

[10] Hubbard, R. F., Spicer, D. S. and Tidman, D. A., Proceedings of the Heavy Ion Fusion Workshop (1978) ANL-79-41, 379.

[11] Thompson, W. B., Proceedings of the Heavy Ion Fusion Workshop (1978) ANL-79-41, 147.

[12] Burke, R. J., Proceedings of the Heavy Ion Fusion Workshop (1978) ANL-71-41, 5.

[13] Moses, G. A., Conn, R. W., Abdel-Khalik, S. I., Cooper, G. W., Howard, J., Magelssen, G. R., Proceedings of the Third Topical Meeting on the Technology of Controlled Nuclear Fusion, Vol. 1 (1978) 448.

[14] Blink, J. A., Walker, P. E., and Meldner, H. W., Trans. Am. Nucl. Soc., 27 (1977) 71.

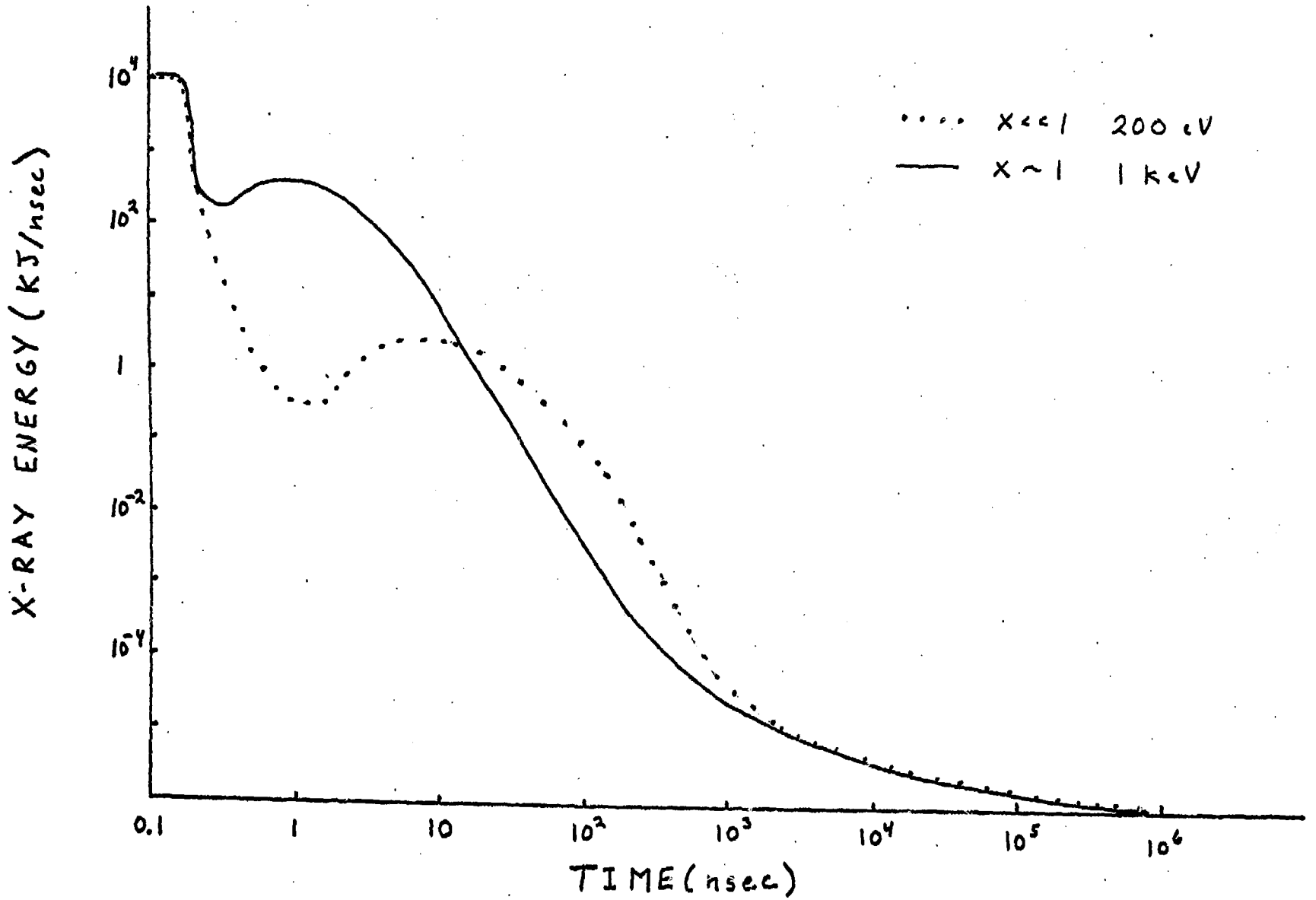

Fig. 1 Time plots of the x-ray energy incident upon the first wall of a five meter radius spherical chamber filled with 100 Torr of neon.

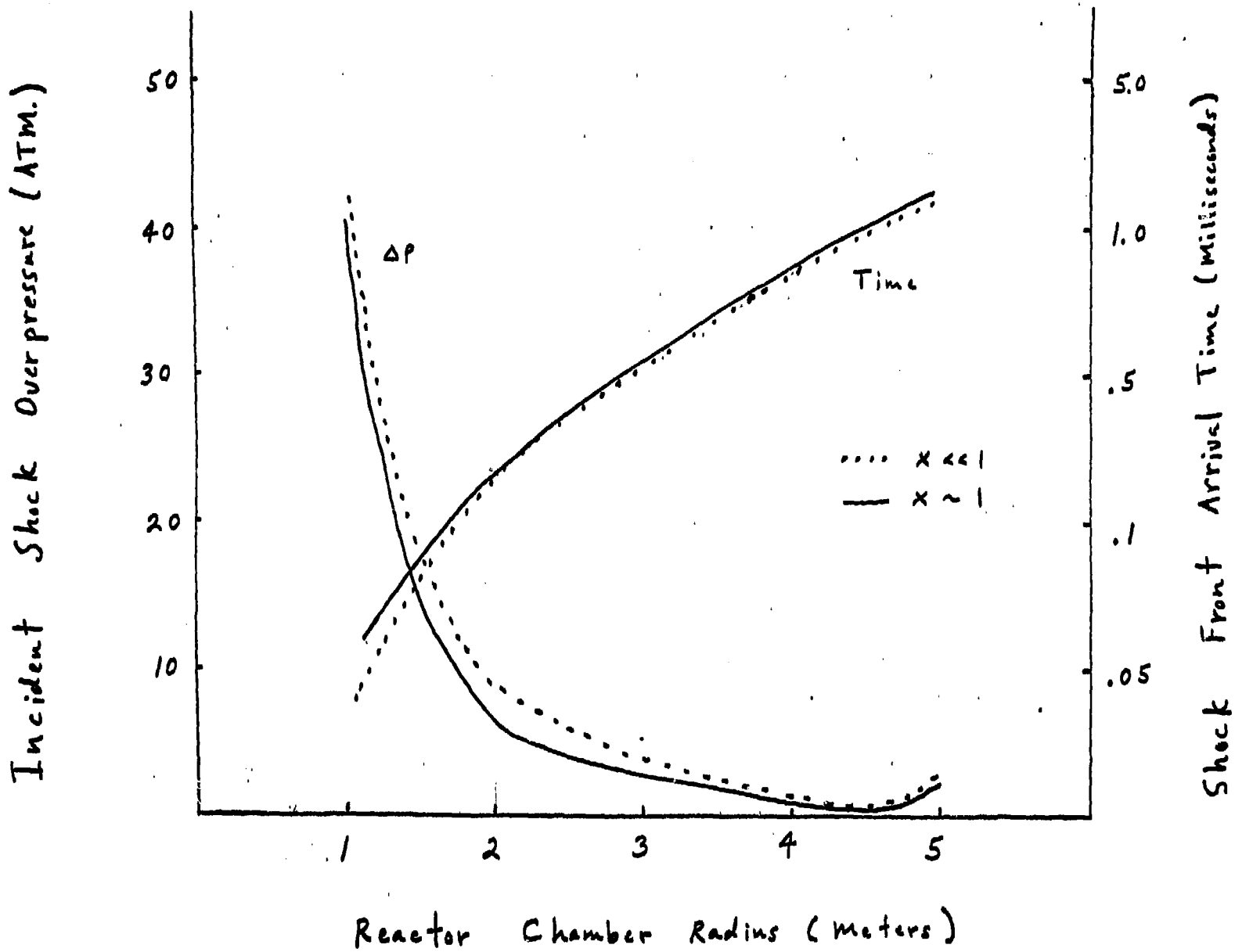

Fig. 2 Plasma overpressure and arrival time vs radius for a 5 meter chamber filled with 100 Torr of neon.

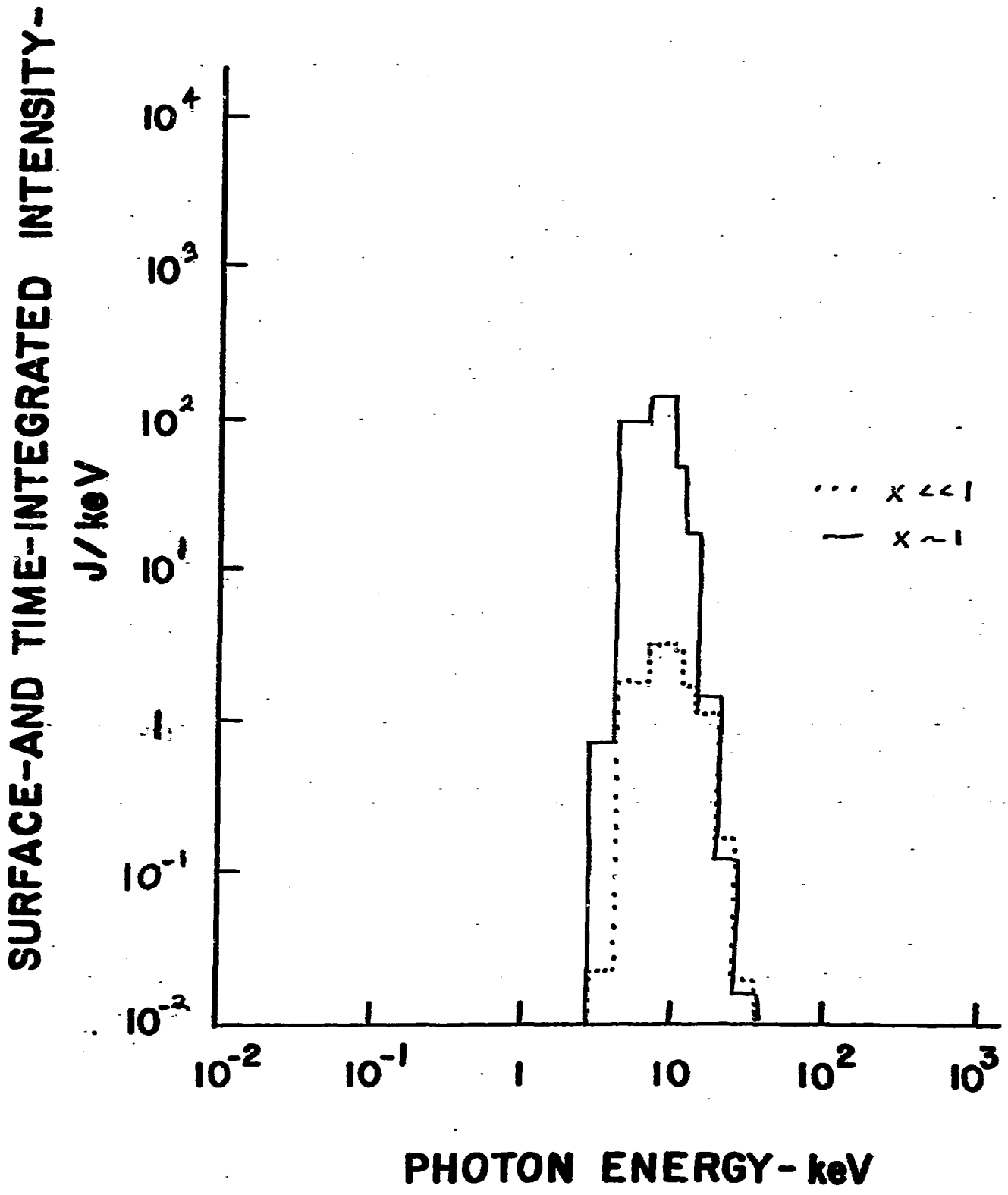

Fig. 3 Time integrated x-ray spectra incident upon the first wall of a 5 meter chamber filled with 100 Torr of neon.

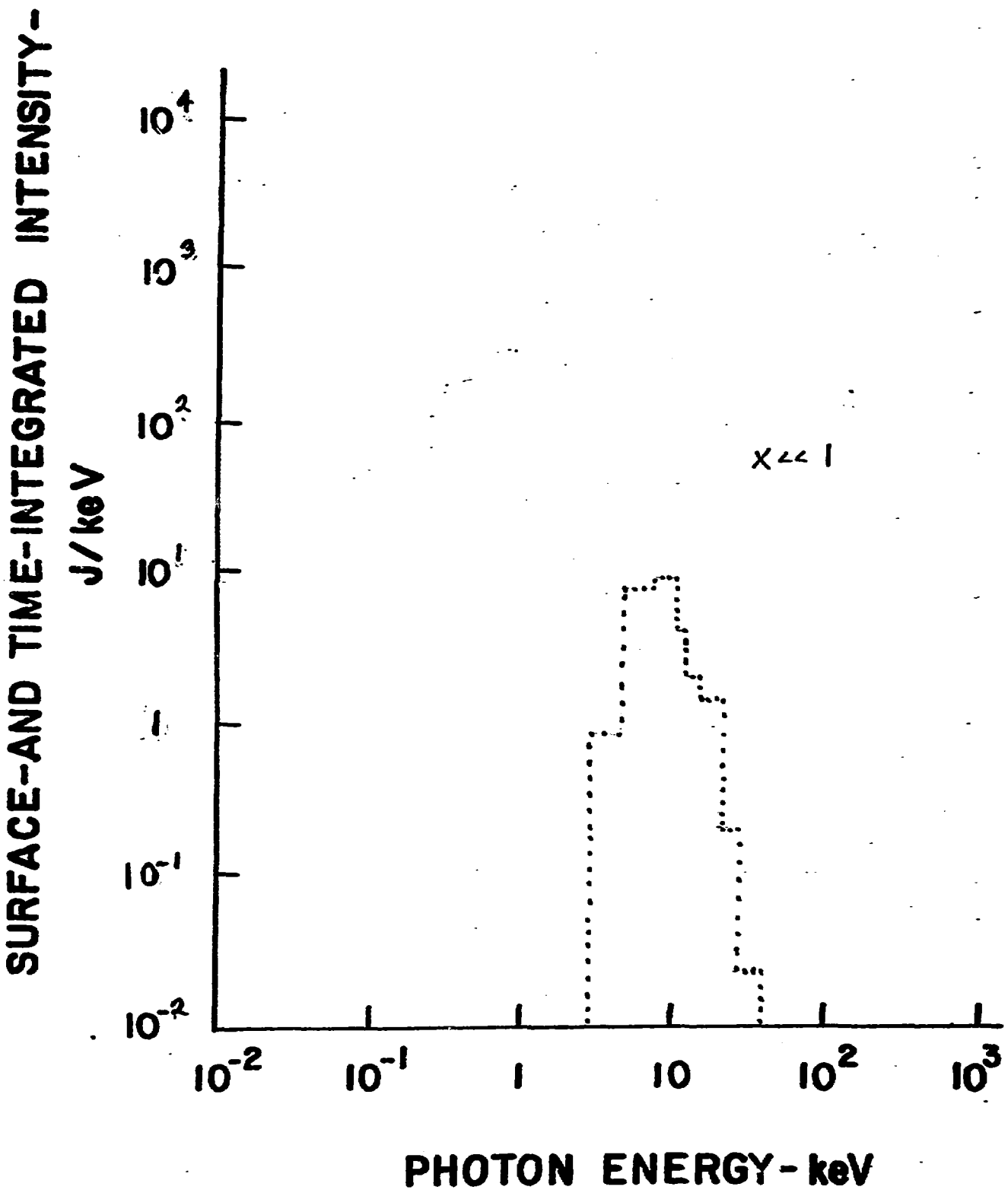

Fig. 4 Time integrated x-ray spectrum incident upon the first wall of a 3 meter chamber filled with 100 Torr of neon.

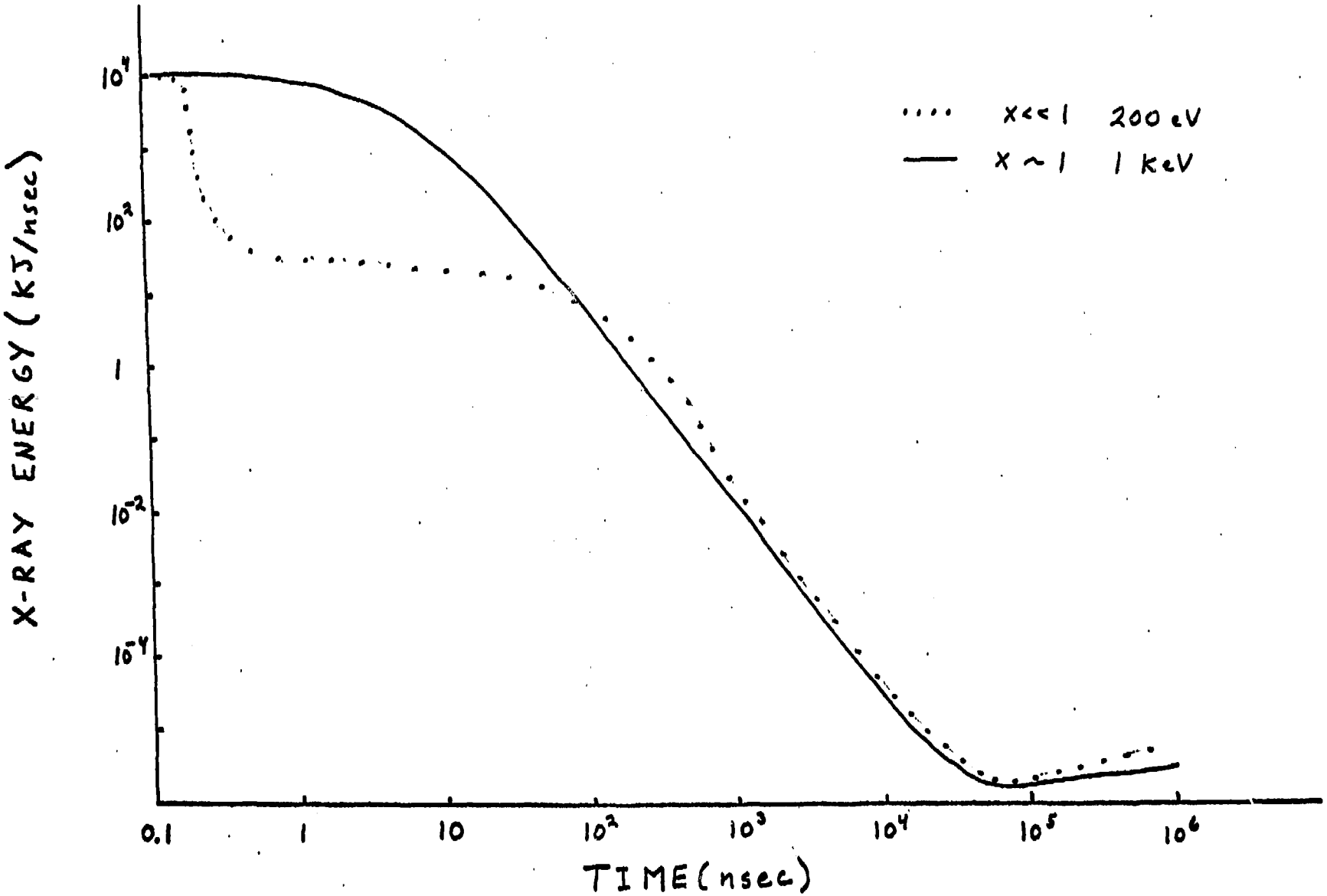

Fig. 5 Time plots of the x-ray energy incident upon the first wall of a five meter radius spherical chamber filled with a Torr of neon.

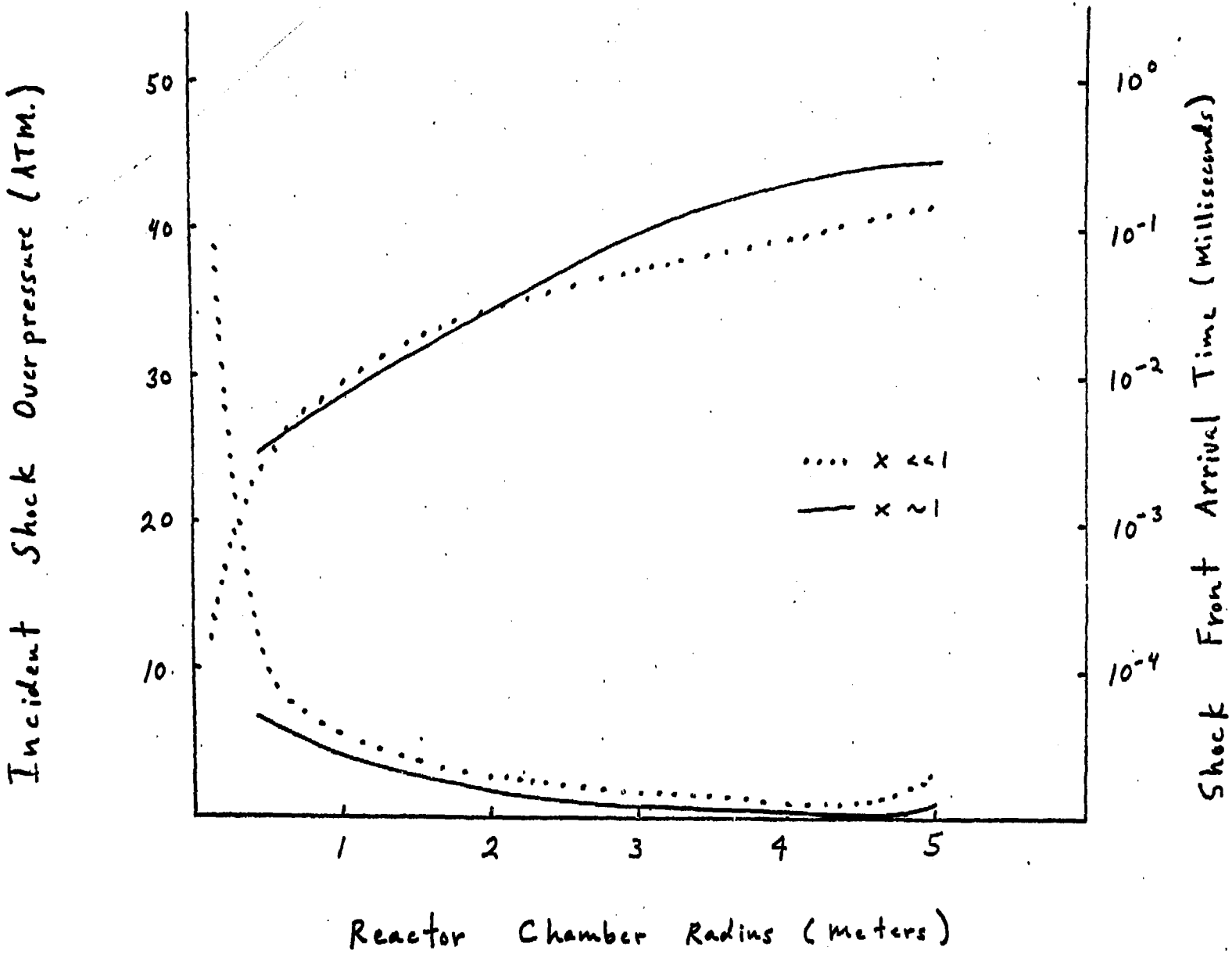

Fig. 6 Plasma overpressure and arrival time vs radius for a 5 meter chamber filled with a Torr of neon

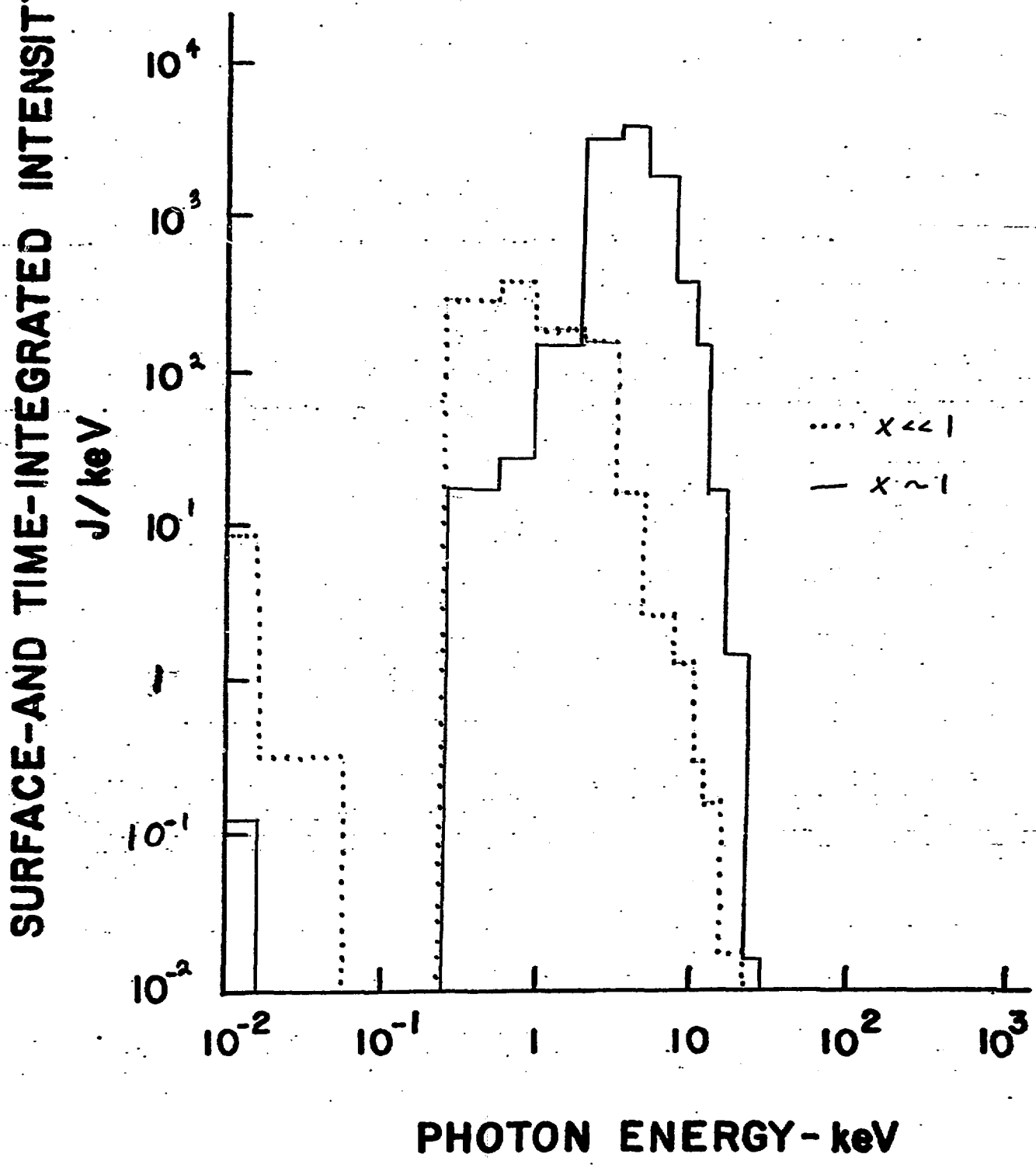

Fig. 7 Time integrated x-ray spectra incident upon the first wall of a 5 meter chamber filled with a Torr of neon

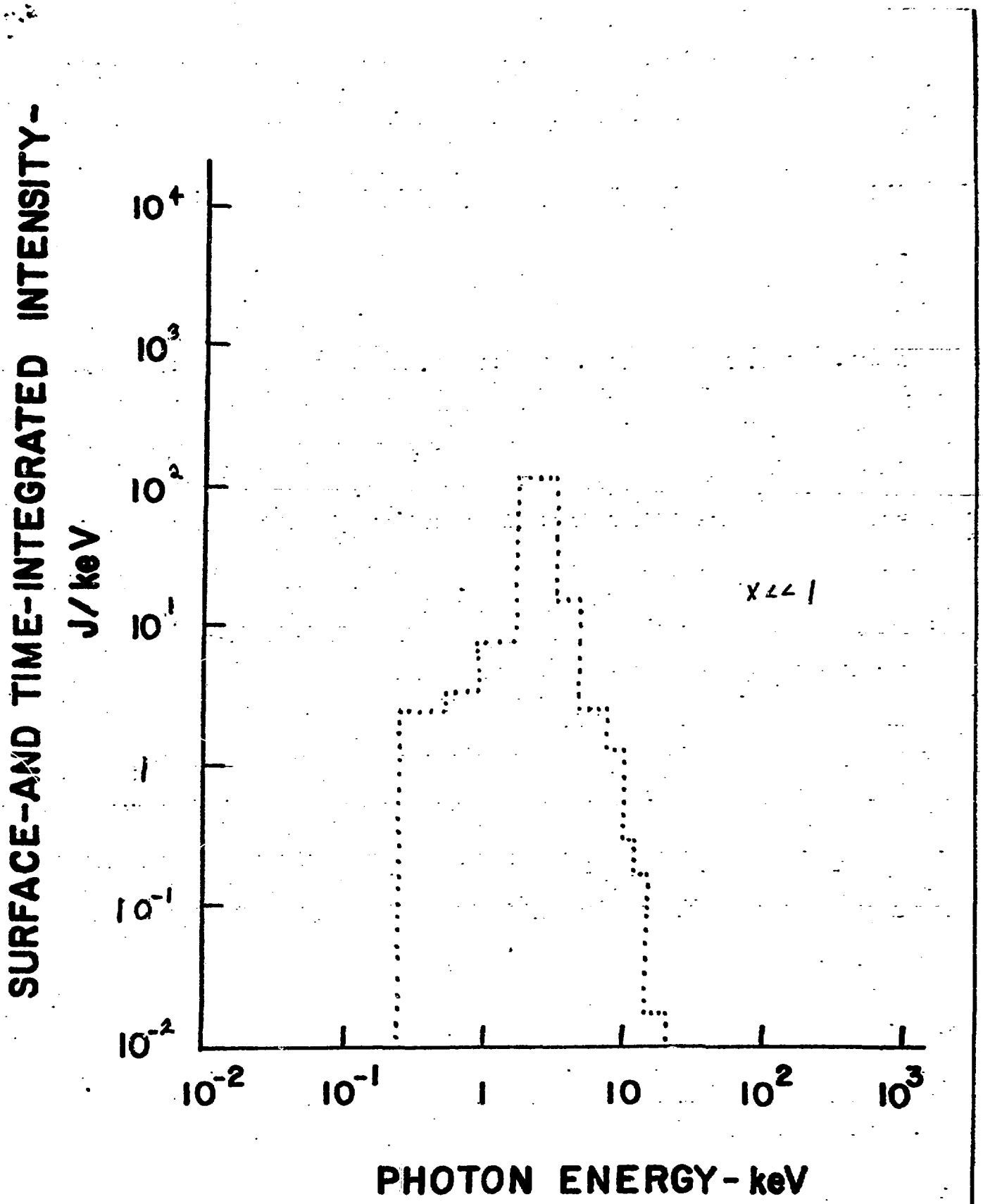

Fig. 8 Time integrated x-ray spectra incident upon the first wall of a 10 meter chamber filled with a Torr of neon